Experimental Techniques (2021) 45:601–612
https://doi.org/10.1007/s40799-021-00444-6

RESEARCH PAPER

Experimental and Numerical Investigation of Process Parameters on the Residual Stresses in the Al-Cu FGM Materials

A. Gheysarian [1] · M. Honarpisheh [1]

Received: 30 April 2020 / Accepted: 18 January 2021 / Published online: 9 February 2021

Abstract

Functionally gradient materials (FGM) are new materials that can offer different properties depending on the structure. In this study, two aluminum and copper powders were combined together by the rules of FGM materials. When two different materials are combined in the structure of the FGM, due to the difference in the thermal expansion coefficients of these two materials, residual stresses are created in the sample. The results of residual stresses measurement were compared with done studies in the past as well as their results. Due to the compressive nature of the FGM manufacturing operations, the measured results show the creation of compressive residual stresses in the structure of the constructed samples. The obtained maximum amount of residual stress from the experimental sample was 130 MPa. Also, a finite element model (FEM) was used to evaluate the residual stresses in the structure of the FGM. The experimental measurements were validated by finite element simulation, which presented a good agreement with an error of 4%. Finally, the effects of pressure values in the powder pressing, layout and heat treatment temperatures were investigated by the FEM.

Keywords Functionally gradient materials · Al-cu · Residual stress · Contour method

Introduction

The concept of FGMs was introduced by Japan in the 90's for use in the aerospace industry [1]. The development and research of these materials, due to their structural and interior properties such as electrical conductivity, heat transfer, etc., led to their use in nuclear fields, reactors, medical engineering, piezoelectric devices and biological systems. For example, biological systems are among the applications of FGMs. In biological usage, each layer plays a specific application. The structural slope of the materials in a functionally graded sample creates different internal properties that by changing the slope and amount of each material in each layer can create different structures and characteristics [2–5]. FGMs are an expanded sample of composites, in which different materials combine according to a specific volume fraction and give rise to new graded properties [6]. In the FGMs, several materials combine with different thermal expansion coefficients that this feature causes residual stresses in the structure of these materials [6]. The idea of FGM originate from composite materials, which combine two or more different constituents and exhibit good material properties [7]. FGMs are manufactured in a variety of ways, including powder metallurgy [8], centrifugal casting [9], steam deposition [10], and so on. Using powder metallurgy for manufacturing the FGMs, includes the composition of the powder material base on the specific weight percentage, compression by the press and sintering operations [11]. There are several ways to classify FGMs. Depending on how the layers are graded, FGMs can be classified as stepwise FGMs or continuous FGMs. FGMs can also be classified into compositionally FGMs and structurally FGMs [12]. Zhang et al. [13] deposited functionally graded Ti-6Al-4 V/Titanium carbide (TiC(by laser metal deposition (LMD) with stepwise gradient: 10% TiC, 20% TiC and 30% TiC. The variation of hardness along the compositional gradient was studied. Vickers hardness changed from 300 HV1.0 at the Ti-6Al-4 V bottom substrate to 600 HV1.0. Zhang et al. [14] Manufactured of Ti- TiC FGM by LMD method. Different laser parameters were applied in different layers according to the variation of material composition. The hardness of the Ti-40vol %TiC FGM increased smoothly with the TiC concentration and no obvious interface was observed.

✉ M. Honarpisheh
honarpishe@kashanu.ac.ir

[1] Faculty of Mechanical Engineering, University of Kashan, Kashan, Iran

Mahamood et al. [15] fabricated Ti-6Al-4 V/TiC FGM with composition of 100% Ti-6Al-4 V to 50% Ti-6Al-4 V/50% TiC. Wear volumes for made samples were tested and compared with fixed and optimized parameters. It was discovered that optimized parameters can result in better wear resistance. The relationship between tensile properties and TiC volume fraction studied by Li et al. [16]. The ultimate tensile strength (UTS) of Ti-6Al-4 V/TiC FGM with 5%TiC volume fraction was enhanced by about 12.3%. Yang and Troczynski [17] used a non-pressure sintering method and sol-gel processing to produce FGMs with a maximum voltage of 60. However, due to limitations and high porosity, this method was not suitable for the manufacturing the FGMs. In this system, when the percentage of silicon carbide increased from 5 to 50, the porosity increased and also due to the direct contact of silicon carbide grains, the density of the composite decreased, which is one of the weaknesses of this system. Experiments on Silicon Carbide)SiC(FGM by Sohda et al. [18] showed that the porous structure had better resistance to breakdown and delamination than the dense structure, while the dense structure had a higher level of local stresses. Finot et al. [19] stated that the micro-structural details should be carefully examined to study the distributions of stresses in FGM. Kim and Noda [20] used a laminate theory to analyze three-dimensional transient temperatures in FGM materials. Ootao and Tanigawa [21] considered a functionally graded (FG) plate as a plate consisting of several layers and defined different properties for each layer. Reiter et al. [22–24] carried out detailed finite element studies on the discrete and homogenized models of FGM that discrete model simulated skeletal and particulate micro-structure and homogenized models in which the effective properties were applied by the Mori–Tanaka method. The results of the comparison of these two models are presented. Attempts were made to analyze 3D transient temperature distribution and thermal stresses on FG plates. Cheng and Batra [25] used the asymptotic expansion method to investigate the three-dimensional thermal deformation of the elliptical plane of the FG material. Yang and Shen [26] investigated the initial stresses of FG- plates and provided a free and forced vibrational analysis, based on the high-order shear deformation theory in a thermal environment. Recently Vel and Batra [27] presented a detailed three-dimensional solution for mechanical vibrations and thermal stresses on a simply supported rectangular FG plate. Vel and Batra [28] investigated thermoelastic cylindrical bending deformations in FG plates and provided a detailed solution. They also stated that, due to the large transient thermal stresses than steady- state stresses, quantitative analysis of stresses in the design of FG plates is very important. So far, many studies have been carried out on the thermal stresses in FG plates base on the theory of these plates.

For the first time, FGM consisting of ceramic and metal were used as thermal coatings in aerospace fields. Originally, pure ceramic materials were used for the coatings, which caused destructive residual stresses due to the thermal mismatch and different thermal expansion coefficient with the base metal. In the manufacturing of FGMs, different thermal properties, heat treatment as well as subsequent cooling of the constituent particles cause many problems that lead to destructive residual stresses. To produce FGM materials without cracking and breakage between layers, it is important to consider and to check that residual stresses are minimize and uniformly distribute between layers. The extent and impact of residual stresses on the performance of FGM materials are very important. Therefore, it is important to study the amount, type and distribution of residual stresses in these materials. Residual stresses are self-equilibrium stresses that remain in the component and cause irreparable damage over time. Residual stresses accumulate with external loads and breaking or damaging the final sample or destroying its dimensional accuracy. For this reason, it is important to control residual stresses by controlling the methods of fabrication or de-stressing the final components. Depending on the applications, there are different methods for measuring residual stresses such as hole drilling [29], slitting method [30], ring core method, [31], X-Ray method [32] and contour method [33]. Shaw [34] examined the effects of different material combinations including the compositional gradient, elastic modulus, coefficient of thermal expansion and the number of layers on the rate of thermal residual stresses in FGMs and presented the results. Shabana et al. [35] by using the finite element method, examined thermal residual stresses on the FGM plate, when the plate is subjected to three types of temperature conditions by using microscopic combination law. Grujicic et al. [36] examined the effects of thermal residual stresses on the 316 stainless steel/alumina FGM and expressed the optimization conditions of this process. Becker et al. [37] examined the number of residual stress in the FGM. In this study, the effects of thermal operations on the amount of residual stresses were expressed numerically. Lee et al. [38] looked at the effects of layers on residual stress in FGMs. In this study, the effects of the number of layers 3 to 20 were investigated and the finite element method was used to verify the experiments. Wei et al. [39] by using changes in how the layers are distributed, optimized the number of residual stresses in the Ni/Al_2o_3 FGM. Dancer et al. [40] conducted an experimental study of how to distribute residual stresses in the Alumina-Silicon Carbide FGM and verified the experiments by using finite element method. Ding et al. [41] investigated FGM residual stresses and tried to optimize and reduce the number of residual stresses by changing the composition of the ingredients. Parihar et al. [42] used a novel analytical model to predict the amount of thermal residual stresses in sigmoid FGMs. In this paper, the effect of sigmoid function graded profile on residual stresses was investigated. Shi et al. [43] examined the extent of residual stresses in the bonding of

ceramic and titanium FGM and compared the experimental and simulation results by using finite element simulation. Alexandrov et al. [44] examined the distribution of residual stresses in the FGM disk, under the influence of internal pressure. Strashnov et al. [45] examined the distribution of residual stresses in the FGM disk under the influence of external pressure. Wagih et al. [46] studied the composition of alumina and copper, as well as the methods of composition and its results. In this study, dry mixing, mechanical alloying and mechanochemical methods were examined. The results indicated that according to the hardness and other considered parameters, dry mixing and mechanical alloying techniques were the most appropriate methods for producing this combination of materials. Eltaher et al. [47] produced the Al-Mg/Al_2o_3 dual matrix nanocomposite and investigated the correlation between powder morphology, crystalline structure and mechanical and tribological properties. The results showed that magnesium milling with Al_2o_3 particles in the initial stage before mixing with Al had a good dispersion of Al_2o_3 nanoparticles in the dual matrix of Al-Mg. In this paper, Fathy et al. [48] by using electroless deposition technique, investigated the effects of combinations Al with two Ni-coated Al_2o_3 ceramics and Ni-coated graphene nanoplatelets (GNPs) to form Al-Al_2o_3/GNPs hybrid nanocomposite (and) with improved mechanical and wear properties, compressive strength, hardness, wear properties and coefficient of friction. The results showed that increasing the volume fraction of GNPs increased the compressive strength, hardness and anti-friction properties of composites. In this study, Wagih et al. [49] produced Al–Al_2o_3 nanocomposites. This work provided an efficient technique for improving the compressibility and thermal properties of Al-Al_2o_3 nanocomposites. The results showed that the addition of Al_2o_3 to the Al matrix increased the compressibility behaviour of the produced nanocomposite. Abd-Elwahed et al. [50] made Cu–ZrO2/GNPs nanocomposites. In this article, the effect of GNPs mass fraction of, 0, 0.5, 1 and 1.5, was investigated on the mechanical and electrical properties of the produced nanocomposite while keeping the ZrO2 mass fraction constant at 5%. The results showed that compressive strength increased with GNPs content. The result indicated an efficient production process for high strength and good conductivity, which were used in many structural applications. Sadoun et al. [51] produced Cu–ZrO2/GNPs hybrid nanocomposites by using powder metallurgy technique. In this article, the effect of GNPs mass fraction of, 0, 0.5, 1 and 1.5, was investigated on the mechanical and tribological properties while keeping the ZrO2 mass fraction constant at 5%. In this study, Sadoun et al. [52] investigated the mechanical and tribological properties of Cu–Al_2o_3 nanocomposite hybridized by silver (Ag) coated graphene nanoplatelets (GNPs). In this study, four different contents of GNPs, 0.3, 0.6, 0.9 and 1.2 wt.% were considered to highlight its effect on the properties of the produced nanocomposite. The results showed a significant improvement in hardness by increasing the content of GNPs to 55.2% compared to pure copper due to grain refinement, high strength of GNPs and strengthening grain boundaries by GNP precipitation. Abu-Oqail et al. [53] studied the effect of silver impregnated GNPs on the microstructure and mechanical properties of Cu-Fe dual-matrix nanocomposite. One of the most important factors in the production of Cu-Fe dual matrix nanocomposites with improved properties was to prevent the dissolution of iron in copper. For this purpose, GNPs electroless coated Ag was used for the production of Cu-20%Fe/GNPs nanocomposite with improved mechanical, physical and wear properties. The results showed that hardness of Cu-20%Fe/0.6%GNPs nanocomposite improved by 12.5% compared to Cu-20%Fe dual-matrix composite. Ahmed et al. [54] investigated the effect of GNPs content on the thermal and mechanical properties of a new combination of new hybrid Cu-Al_2o_3/GNPs coated Ag nanocomposite. In this study, Hybrid Cu-Al_2o_3/GNPs coated Ag nanocomposites with GNPs content of 0%, 0.3%, 0.6%, 0.9% and 1.2% were successfully produced with well improved in mechanical, electrical and thermal properties and compressive strength, hardness, thermal and electrical properties. The results showed that the compressive strength and hardness improve with increasing GDP achieving 88.1% and 55.2%, respectively. Aghaei et al. [55] investigated the effect of the cooling system on mechanical properties and residual stresses in AISI 1045 steel in cooling the sample after heat treatment. In this study, the contour method was used to measure residual stresses. The results indicated that the highest hardness as well as the highest compressive residual stresses were obtained in water cooling. Nazari et al. [56] Investigated the effect of stress release by annealing process on the microstructure, mechanical properties and number of residual stresses in copper sheet in the constrained groove pressing process. In this process, the contour method was used to measure the amount of residual stresses.

In this study, the contour method is used to measure residual stresses in fabricated samples. So far, many studies have focused on the importance of joining two or more different materials in a single mould, to improve properties and prevent failure between layers. Therefore, the purpose of this study is to investigate and optimize the structural properties of the FGM, as well as to evaluate and minimize the number of residual stresses to improve sample performance.

Experiment Procedure

FGM Material Production

In this study, powder metallurgy method was used to produce a sample of FGM. This process involves the preparation of powder material, layering, pressing and heat treatment. In

FGMs, the volume fraction of each material varies by layer, which changes the properties in this regard. Accordingly, aluminum and copper powder were prepared in the same size and were layered inside the mould. It is important to note that the non-uniform size of the powders causes residual stresses in the final sample. The pre-designed mould was then compressed by the press and the final sample was transferred to heat treatment furnace (Fig. 1).

Mould design is one of the most important parameters in this process. The used mould in this test must be of sufficient strength and designed and constructed in such a way that the final sample can be removed easily. For this reason, after several attempts and errors, the mould was made of CK45 (Fig. 2). In this design, due to the designed angle at the end of the mould, the sample removed easily after the compression process.

Heat treatment is one of the affecting factors on the dimensional quality and amount of residual stresses in the finished samples. FGMs consist of two or more materials with different properties. Different thermal conductivity and thermal expansion of constituents cause dimensional problems in the final sample (Fig. 3). Therefore, selecting the appropriate heat treatment process in making FGMs is very important. Produced sample is a disk with 50 mm diameter and 12 mm thickness.

In this study, after several tests with pressures of 100 tons and above and also checking the quality of the produced sample, the pressure of 350 tons was used to compress the samples. Produced samples by the pressure of 350 tons were subjected to several stages of heat treatment under different conditions. Finally, a sintering temperature of 900 °C was used for these experiments. To perform sintering operation, the sample was kept at 400 °C for 100 min and then at 900 °C for 150 min and then was cooled in a furnace for 24 h. It is important to note that sintering temperature and pressure were obtained with a lot of trial and error to achieve the appropriate quality.

Residual Stress Measurment by the Contour Method

Contour method is one of the residual stresses measurement methods. In this measurement method, which is one of the destructive measurement methods, the amount of residual stresses in a sample is measured by calculating the released strains [57]. The contour method involves sample cutting, strain measurement, data processing and finite element simulation. Cutting the sample is the most important step in this process. This process should be done by a wire electric discharge machine (EDM). In this study, the prepared samples were cut with a high precision wire cutter (CHARMILLES ROBOFIL 290 wire EDM machine) (Fig. 4). Made incision at this stage should be smooth and clean and not cause any plastic deformation. Cutting conditions and parameters must be selected in such a way that they do not affect the measurement of residual stresses. After cutting a sample, controlling the temperature to prevent the generation of residual stresses is another important point. The measurement of the sample surface deformations is the next step of this process. After cutting the sample, the strains released to the cutting surface and produced a deformation that was measured by a coordinate measuring machine (CMM) (Sky 1). The accuracy of this device is too important. Accuracy of the used device in this study was 0.0001 mm at the site where the residual stresses were measured. The CMM has a measuring probe that contacts the sample surface and reports the coordinates. The accuracy of the measurement depends on the number of inspected points, which specified by the operator. According to the other

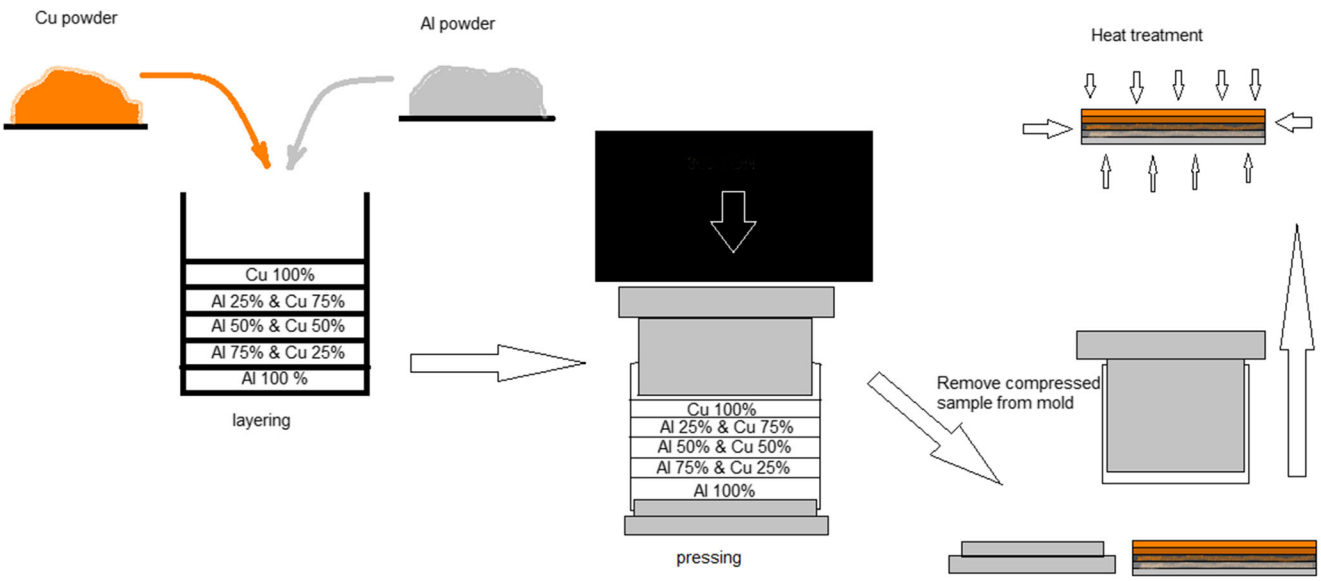

Fig. 1 Schematic of powder metallurgy process of FGM materials

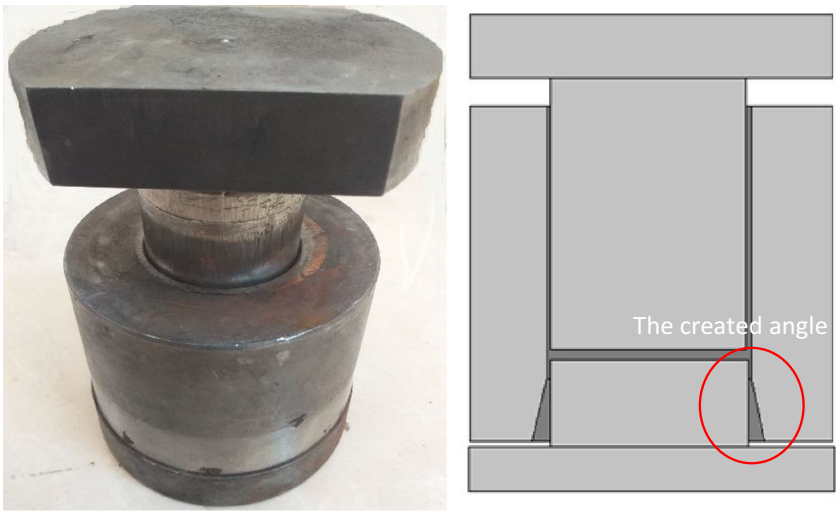

Fig. 2 Used mold and schematic of design mold

readings [58, 59], in order to improve measurement accuracy, the points were measured at a distance of 0.5 mm.

It should also be note that the released strains from the two surfaces must measured. The two-level strain was measured and mediated and reported as released strain due to residual stresses. In this study, 100 points were measured in the X direction and 24 points in the Y direction, which included a total of 2400 points. The released stresses were measured as strain by a CMM machine and transferred to MATLAB software. The Polynomial model was used to fit a surface to the coordinate data. The used polynomial model had a coefficient of 4 in the X direction and 5 in the Y direction, which showed the best possible case with 78% compliance. Fited graphs on these points (Points that the coordinates of them were specified by the transient plane of the X and Y axes) (Fig. 5) and the equation of these graphs was provided by MATLAB software.

Even under the best cutting and measuring conditions, there were some defects in the measured points that can be considered as errors which can be omitted from the data sets by using regression. At this stage, the desired sample was modelled in ABAQUS (Fig. 6).

Finite Element Simulation

The following steps were performed to simulate the distribution of residual stresses in the FGMs. The generated sample was modelled in the software, layer by layer. Then, the attributes of each layer were defined in the properties section. The properties of each layer must be introduced separately into the software. To did this operation, the properties of each layer (such as E) were expressed, depending on the weight percent of the used material in that layer. Thus, the following should be done for each layer, if the FGM layering was based on equation (1) or any other equation.

$$V_{material1} = \left(\frac{2Z+h}{2h}\right)^{N} \tag{1}$$

$$\sum V_i = 1 \rightarrow V_1 + V_2 = 1 \tag{2}$$

$$\begin{aligned} &E_{each\ layer} = E_{material1} * V_{material1} + E_{material2} * V_{material2} \\ &\rightarrow E_{each\ layer} = E_{material1} * V_{material1} + E_{material2} * (1 - V_{material1}) \\ &\rightarrow E_{each\ layer} = (E_{material1} - E_{material2}) * \left(\frac{2Z+h}{2h}\right)^{N} + E_{material2} \end{aligned} \tag{3}$$

For functionally materials, the properties of each layer (such as α) were defined as the following equations, if the volume fraction of each layer was defined as a polynomial function V (X).

$$\begin{aligned} &V(x) = \sum_{i=0}^{n} V_i x^i = v_0 + v_1 x^1 + v_2 x^2 + \\ &\alpha = \alpha_1 + (\alpha_2 - \alpha_1) * v = \alpha_1 + \Delta\alpha v \end{aligned} \tag{4}$$

$$\rightarrow \alpha(x) = \alpha_1 + \ v_0 \Delta\alpha + \sum_{i=0}^{n} \Delta\alpha V_i x^i \tag{5}$$

Based on the above proven equation, the properties of each layer were calculated and defined in the material properties section of ABAQUS software (Table 1).

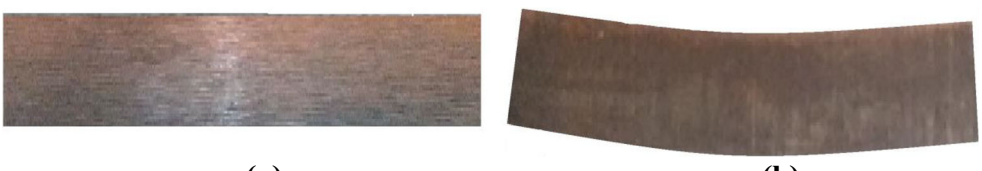

(a) **(b)**

Fig. 3 Effects of heat treatment on dimensional quality of samples (a) Well dimentional sample (b) Failed sample

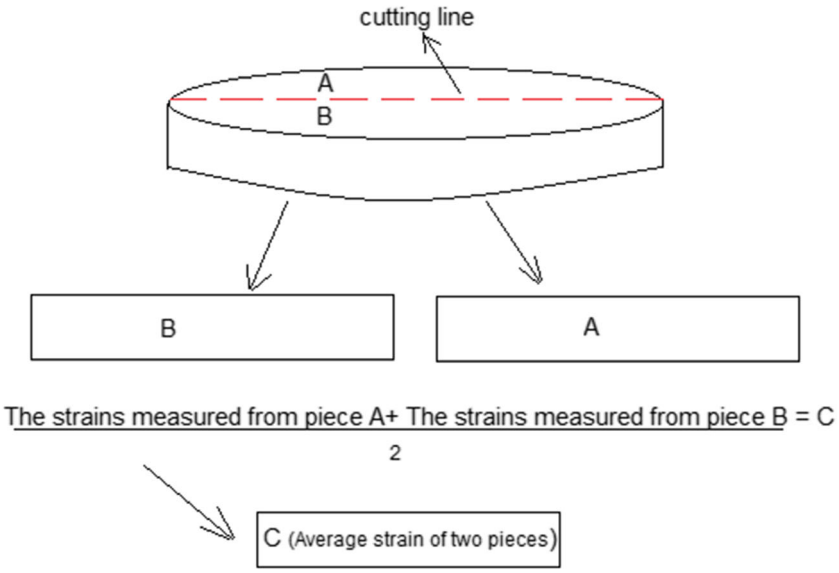

Fig. 4 Schematic of the surfaces on which the released strains are measured

Garson porous material model was used to simulate the metal powder in the ABAQUS. Using this model is very important because of the different behaviour of powder and metal. Due to the presence of voids in materials with pores, the degree of plastic deformation depends on the amount of applied pressure.

$$\Phi = \left(\frac{q}{\sigma_y}\right)^2 + 2q_1 f\cosh\left(\frac{-3q_2 p}{2\sigma_y}\right) - \left(1 + q_3 f^2\right) = 0 \qquad (6)$$

The Garson model operates base on equation (6). All the parameters in this equation except *f* were based on the properties of the material (q is the effective Mises stress, p is the hydrostatic pressure, σy is the yield stress and q_1 , q_2, q_3 are material parameters (For typical metals, q_1= 1 to 1.5, q_2= 1.5, q_3= q_1^2= 1 to 2.25. But the original Gurson model is obtained when the values of all these three parameters are equal to 1. These values can be expressed as a tabular functions of temperature and/or field variables. In this study, for simplification, the values of these 3 parameters were considered equal to 1.)). *f* indicates the porosity status of the material in question. When *f* equals zero, it denotes non-porous and *f* equals one denotes that matter is fully porous. After modelling the FGM in ABAQUS software, obtained equation from MATLAB software was applied as loading to the model surface in ABAQUS. In the final step, the model was meshed and then the analysis was performed. This model consists of 12,325 C3D8R elements that were outlined in linear hexagons. After performing the simulation, the residual stresses in the sample were measured (Fig. 7).

In the contour method, the amount of residual stresses was examined in the cutting plate. Dou to the existing CMM device for this study capabled to measure the amount of variation along the z-axis, the cut-off plate was positioned in this direction and the amount of strain along this axis was calculated (In fact, according to Fig. 4, the z-axis was perpendicular to the cross-sectional area of A and B). Two longitudinal and transverse paths (Fig. 7) were defined in the cross-section, to investigate the residual stresses, and the values of residual stresses for these two paths were determined.

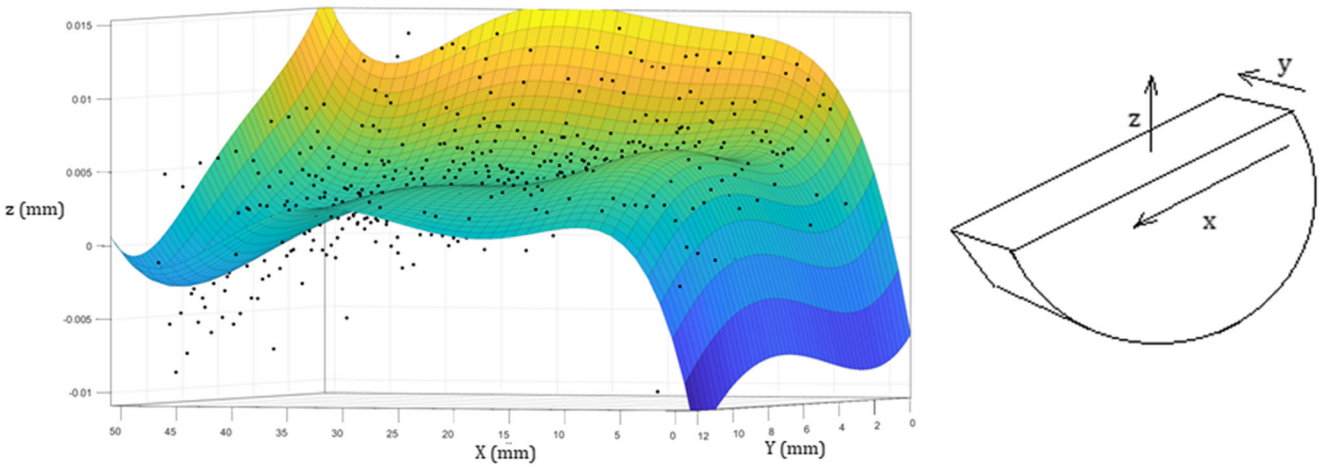

Fig. 5 Fit diagram on the CMM data

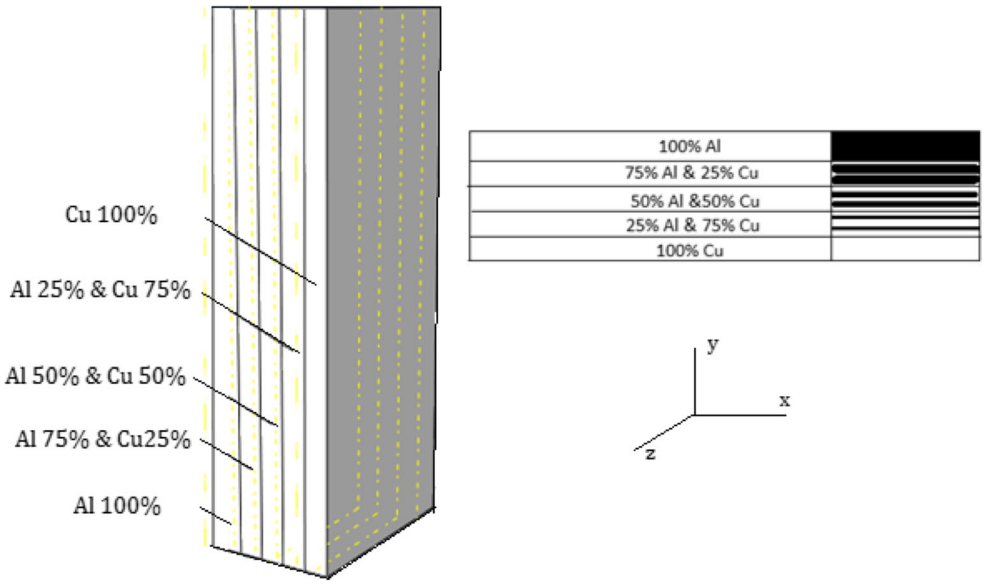

Fig. 6 Modeled sample in ABAQUS

As in the contour method, the amount of residual stresses in two paths were obtained from simulation test in ABAQUS. To simulate the finite element model of FGM product process, all process steps were modelled according to reality. The properties of each layer were applied according to the Table 1. Thermal and compressive loads were applied. (To perform this operation in the simulation process, the change Model Theory (in the Interaction Module) should be used. This option was basically the cutting of a sample from the middle by a wire cutter, which released strains and produced corresponding stresses). The performed simulation in this section was different from the performed simulation in the contour method. In the contour method, the loading was done by applying obtained equation from MATLAB software and its proportional stresses were obtained. While the simulation performed in this section was completely based on the fact of the performed process to made this sample.

Result and Discussion

In important and expensive equipment, due to the destructive effects of residual stress, it is important to check this parameter. Due to the cost of making FGM, it is important to study the number of residual stresses and also to choose the right method to do so. The results of residual stress measurements for longitudinal and transverse paths are visible in Fig. 8 and Fig. 9. The longitudinal path consists of the crossing of one particular layer (point 1 to 2) and the transverse path contains the crossing of all layers and the two ends (point 3 and 4) of this path having two different materials.

As previously stated, Fig. 8 illustrates the residual stresses in the longitudinal section and Fig. 9 illustrates the residual stresses in the transverse section. As can be seen in Fig. 8, the amount of residual stresses increases from the outside to inside the sample. The reason for this happen, is the release of residual stresses in the form of plastic deformation in the outer layers. If the sample has enough time, the residual stresses on the outer layers become zero. The define way for the longitudinal path, crossing from one layer (according to Fig. 8) in the FGM sample and this is because of the symmetry of Fig. 8. Investigation of transverse residual stresses (Fig. 9) in the made sample indicates that tensile stresses creates from the surface (that is in contact with the press) and then these stresses change to compressive stresses. As can be seen the residual stresses at the two outer surfaces of the sample, are tensile and in the middle of the sample, the stresses are compressive. As

Table 1 The properties of each layer

	Young module	Poisson's ratio	Thermal expansion coefficient (α)	Thermal constant (K)	Density	Tensile limit	Modulus bulk
Al	69	0.33	0.000023	220	0.0027	0.35	76
75% Al & 25% Cu	81	0.3325	2.15E-05	253.25	0.004265	0.315	92
50% Al & 50% Cu	93	0.335	0.00002	286.5	0.00583	0.28	108
25% Al & 75% Cu	105	0.3375	1.85E-05	319.75	0.007395	0.245	124
Cu	117	0.34	0.000017	353	0.00896	0.21	140

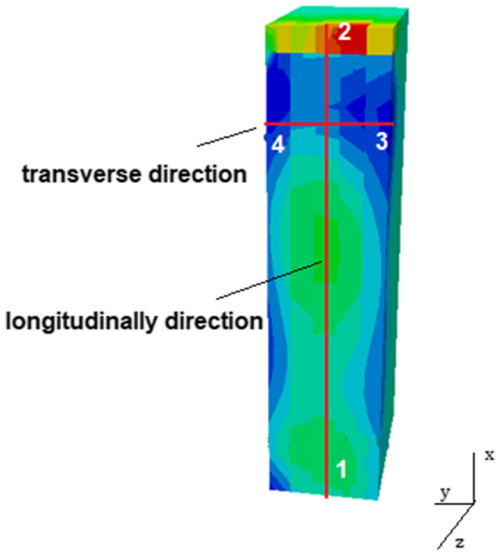

Fig. 7 Defined paths for measuring the residual stresses

can be seen in Fig. 9, totally the residual stress model of the sample is compressive and this is due to the compressive nature of the process. Two sample surfaces have tensile stresses near zero, which the surface in contact with the press having higher tensile stresses than the opposite surface. Another cause of residual compressive stresses is the loss of porosity during the pressure process. The used materials in this process were powders with porosity. The compression of these materials reduces these pores as well as welding the powders to another, causing residual compressive stresses. The reason for the tensile stresses at the sample surface is heat treatment. Two sample surfaces are aluminum and copper that have different thermal expansion coefficients and exhibit non-uniform behaviour at different temperatures. Aluminum is less resistant to copper and more susceptible to tensile deformation than copper and this difference in the two- sample surfaces cause tensile stresses in the two sample surfaces.

The results of residual stresses comparison between simulations and experimental tests are shown in Fig. 10. As is remarkable, there is a good agreement between the experimental results and the simulation, which helps use simulation to obtain some results. The error rate between the experimental and simulation results was about 4%, which was excellent and was obtained by comparing the average amount of residual stresses in the simulation and experimental mode.

Because of the good agreement accrued between simulation results and experimental operations, the simulated model was used to investigate the variation in some of the initial parameters. In this section, the amount of applied pressure to the pressing operation, layout and heat treatment temperature were examined by the simulated model in ABAQUS. Initially, the amount of pressure applied in the pressing operation was examined. To test this parameter, 3 working presses of 120 tons, 300 tons and 500 tons were used. The obtained results were shown in Fig. 11. As can be seen in the figure, the residual stresses increase compressively with increasing pressure. The compressive nature of residual stresses is due to the compressive nature of the operation that already discussed. In fact, exerting pressure on the specimen causes displacement in the body. The resulting displacement, increase the energy in the body, which increases with the pressure and increases the volume of residual stresses. Another reason for the increase in residual stresses with increasing pressure is the compaction of more powder grains and the reduction of pores between them.

To investigate the effect of heat treatment temperature, the process was simulated at temperatures of 700, 1500 and 3000 degrees. The obtained results are shown in Fig. 12. As can be seen in the figure, the residual stresses decrease with increasing temperature. In fact, rising temperatures have improved the conditions. As the temperature increases, the penetration improves and dislocation eliminate and the involved energy in the fragment reduces.

Fig. 8 Residual stress measurement in the longitudinal path

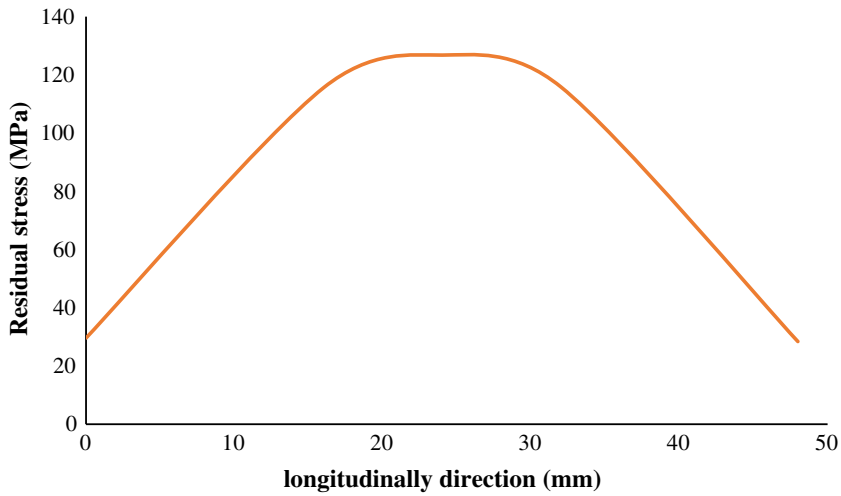

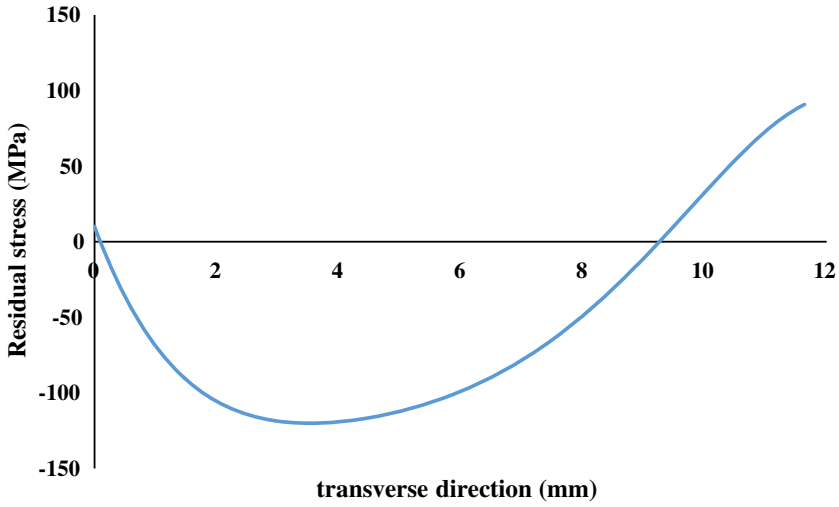

Fig. 9 Residual stress measurement in the transverse path

At low temperatures, due to the lack of heat penetration into the inner layers and the non-uniform deformation, high residual stresses obtaines and as the temperature rises, the heat penetrates into the inner layers and reduces the residual stresses. If the temperature becomes too high, the fragment becomes soft and the residual stresses releases as strain.

Three models were used to examine how the material was layered. In the first model, FGM with 3 layers, in the second

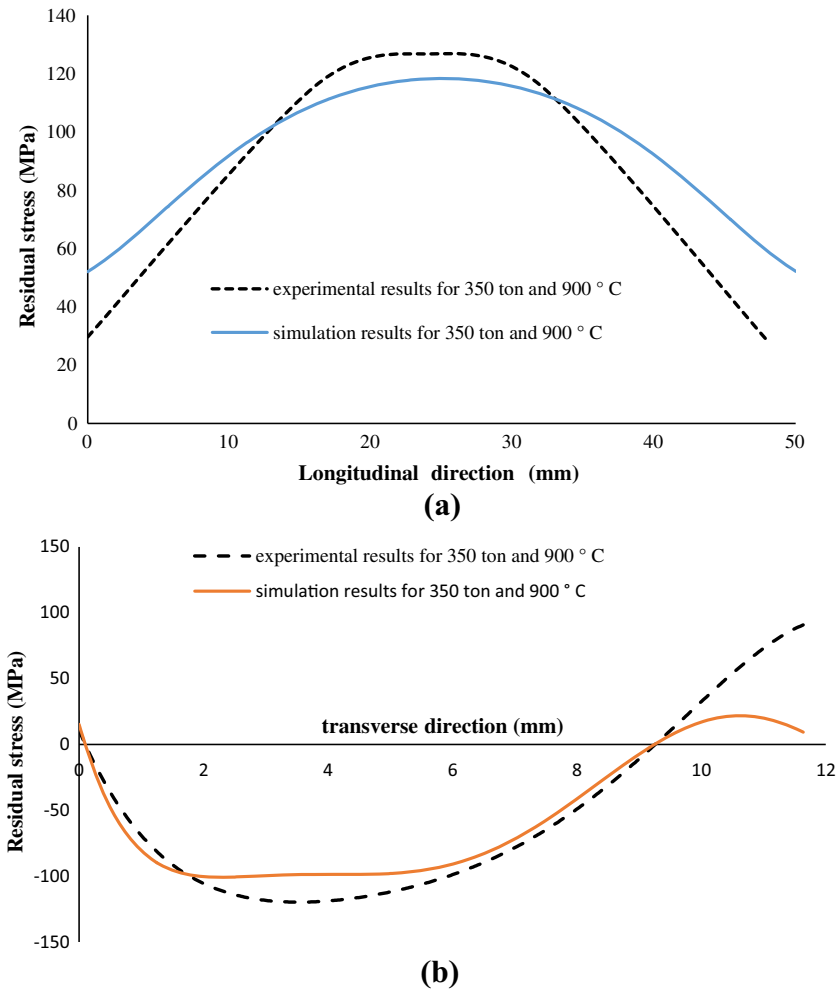

Fig. 10 Numerical and experimental results of residual stress (a) longitudinal path (b) transverse path

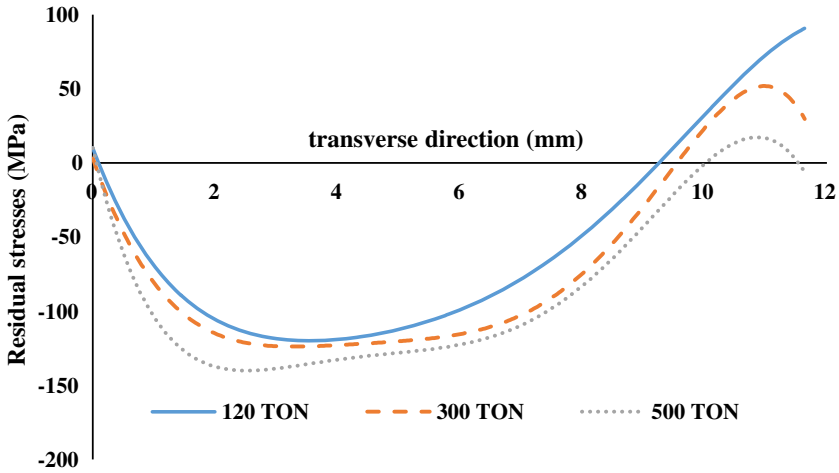

Fig. 11 Effects of pressure values on the residual stress

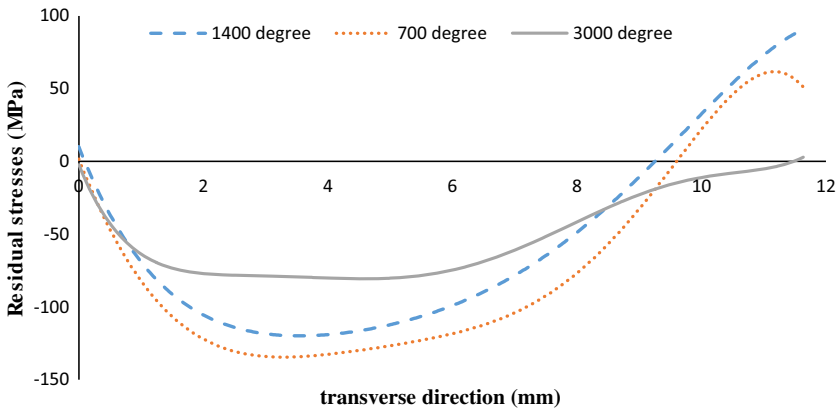

Fig. 12 Comparison results of heat treatment temperature

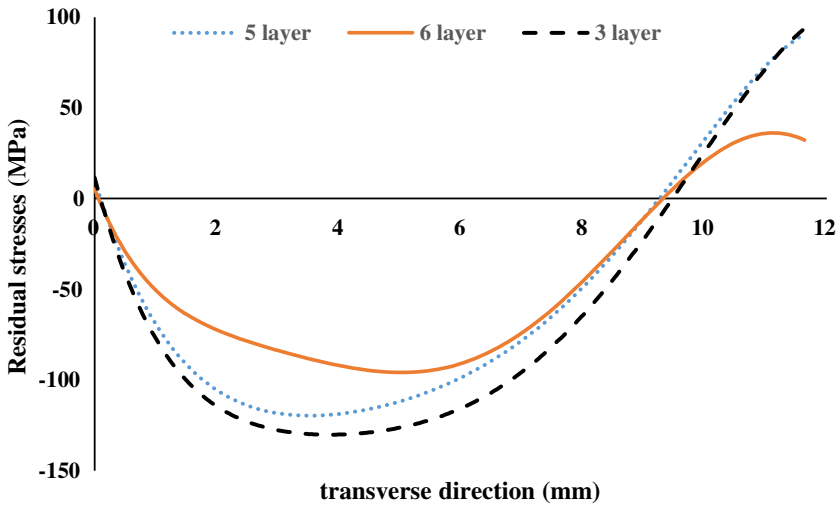

Fig. 13 Effect of layouts number on the residual stress

model with 5 layers and in the third model with 6 layers and the effect of layering on the number of residual stresses was investigated. The results can be seen in Fig. 13. The results indicated that the number of residual stress decreased with the increasing number of layers from 3 to 6. This indicated that the slope of the layout was very influential in the number of residual stresses. Obtained results were consistent with the presented results in Reference [38].

The amount of residual stresses decreases with increasing the number of layers due to greater uniformity of the structure and better communication between the layers, as well as a decrease in the percentage difference between the materials in the layers.

Conclusions

The purpose of this study was to construct an Al-Cu sample and to measure the residual stresses inside it. How these materials were made was very important and it was very influential in the amount of created residual stresses. This section reviews the results of this study.

- One of the most important steps in the powder metallurgy process was heat treatment. Using an inappropriate heat treatment course caused distortion, excessive residual stresses and dimensional damage of the final sample. The FGM has not been given a specific heat cycle due to its consistency of several different materials. Best thermal cycle was achieved by numerous trials and trials for any combination of materials.
- After many trials and errors, the best temperature for this material, according to the final quality control, was considered 900 degrees. The used thermal cycle was to hold the piece for 100 min at 400 degrees and then for 150 min at 900 degrees.
- The number of residual stresses decreased by increasing the heat treatment temperature.
- Due to increasing the uniformity between the layers, the number of residual stress decreased by increasing the number of layers.

Compliance with Ethical Standards

Conflict of Interest The authors declared no potential conflicts of interest with respect to the research, authorship and/or publication of this article.

References

1. Hirano T, Teraki J, Yamada T (1991) Applications of fuzzy theory to the design of Functionally Gradient Materials. In: Transactions of the 11th international conference on structural mechanics in reactor technology
2. Igari T, Notomi A, Tsunoda H, Hida K, Kotoh T, Kunishima S (1990) Material properties of functionally gradient material for fast breeder reactor. In: Proceedings of the First International Symposium on Functionally Gradient Materials, Sendai, Japan, pp 209–214
3. Mattei G, Tirella A, Ahluwalia A (2012) Functionally Graded Materials(FGMs) with Predictable and Controlled Gradient Profiles: Computational Modelling and Realisation. Computer Modeling Eng Sci 87(6):483–503
4. Tani J, Liu G-R (1993) SH surface waves in functionally gradient piezoelectric plates. JSME international journal Ser A, Mechanics and material engineering 36(2):152–155
5. Hirano T (1993) Numerical analysis of efficiency improvement in functionally gradient thermoelectric materials. Functionally Gradient Materials:23–30
6. Suresh, Subra, and Andreas Mortensen. Fundamentals of functionally graded materials. No. BOOK. The Institut of Materials, 1998
7. Campbell, Flake C. Structural composite materials. ASM international, 2010
8. Groves JF, Wadley HNG (1997) Functionally graded materials synthesis via low vacuum directed vapor deposition. Compos Part B 28(1–2):57–69
9. Zhu J, Lai Z, Yin Z, Jeon J, Lee S (2001) Fabrication of ZrO2–NiCr functionally graded material by powder metallurgy. Mater Chem Phys 68(1–3):130–135
10. El-Galy IM, Ahmed MH, Bassiouny BI (2017) Characterization of functionally graded Al-SiCp metal matrix composites manufactured by centrifugal casting. Alex Eng J 56(4):371–381
11. Naebe M, Shirvanimoghaddam K (2016) Functionally graded materials: a review of fabrication and properties. Appl Mater Today 5: 223–245
12. Mahmoud D, Elbestawi MA (2017) Lattice structures and functionally graded materials applications in additive manufacturing of orthopedic implants: a review. J Manufacturing Materials Process 1(2):13
13. Zhang J, Zhang Y, Liou FW, Newkirk JW, Brown Taminger KM, Seufzer WJ (2015) A Microstructure and Hardness Study of Functionally Graded Materials Ti6Al4V/TiC by laser Metal Deposition, p 664
14. Zhang Y, Wei Z, Shi L, Xi M (2008) Characterization of laser powder deposited Ti–TiC composites and functional gradient materials. J Mater Process Technol 206(1–3):438–444
15. Mahamood RM, Akinlabi ET (2015) Laser metal deposition of functionally graded Ti6Al4V/TiC. Mater Des 84:402–410
16. Li L, Wang J, Lin P, Liu H (2017) Microstructure and mechanical properties of functionally graded TiCp/Ti6Al4V composite fabricated by laser melting deposition. Ceram Int 43(18):16638–16651
17. Yang Q, Troczynski T (2000) Alumina Sol-Assisted Sintering of SiC—Al_2o_3 Composites. J Am Ceram Soc 83(4):958–960
18. Sohda Y, Kude Y, Uemura S (1993) Carbon-carbon composites coated with SiC/C functionally gradient materials. Ceram Trans 34:125
19. Finot M, Suresh S, Bull C, Sampath S (1996) Curvature changes during thermal cycling of a compositionally graded Ni Al_2o_3 multilayered material. Mater Sci Eng A A 205(1–2):59–71
20. Noda K-SKN (2001) Green's function approach to three-dimensional heat conduction equation of functionally graded materials. J Thermal Stresses 24(5):457–477
21. Tanigawa YOY (1999) Three-dimensional transient thermal stresses of functionally graded rectangular plate due to partial heating. J Thermal Stresses 22(1):35–55
22. Reiter T, Dvorak GJ, Tvergaard V (1997) Micromechanical models for graded composite materials. J Mech Phys Solids 45(8):1281–1302
23. Reiter T, Dvorak GJ (1998) Micromechanical modeling of functionally graded materials. In: IUTAM Symposium on

Transformation Problems in Composite and Active Materials. Springer, Dordrecht, pp 173–184
24. Reiter T, Dvorak GJ (1998) Micromechanical models for graded composite materials: II. Thermomechanical loading. J Mech Phys Solids 46(9):1655–1673
25. Cheng Z-Q, Batra RC (2000) three-dimensional thermoelastic deformations of a functionally graded elliptic plate. Compos Part B Eng 31(2):97–106
26. Yang J, Shen H-S (2002) Vibration characteristics and transient response of shear-deformable functionally graded plates in thermal environments. J Sound Vib 255(3):579–602
27. Vel SS, Batra RC (2004) Three-dimensional exact solution for the vibration of functionally graded rectangular plates. J Sound Vib 272(3–5):703–730
28. Vel SS, Batra RC (2003) Exact thermoelasticity solution for cylindrical bending deformations of functionally graded plates. In: IUTAM Symposium on Dynamics of Advanced Materials and Smart Structures. Springer, Dordrecht, pp 429–438
29. Sedighi M, Honarpisheh M (2012) Experimental study of through-depth residual stress in explosive welded Al–cu–Al multilayer. Mater Des 37:577–581
30. Kotobi M, Honarpisheh M (2018) Through-depth residual stress measurement of laser bent steel–titanium bimetal sheets. J Strain Analysis Eng Design 53(3):130–140
31. Moazam MA, Honarpisheh M (2019) Ring-core integral method to measurement residual stress distribution of Al-7075 alloy processed by cyclic close die forging. Materials Research Express 6(8):0865j3
32. Nazari F, Honarpisheh M, Zhao H (2020) The effect of microstructure parameters on the residual stresses in the ultrafine-grained sheets. Micron:102843
33. Alinaghian I, Amini S, Honarpisheh M (2018) Residual stress, tensile strength, and macrostructure investigations on ultrasonic assisted friction stir welding of AA 6061-T6. J Strain Analysis Eng Design 53(7):494–503
34. Shaw LL (1998) Thermal residual stresses in plates and coatings composed of multi-layered and functionally graded materials. Compos Part B Eng 29(3):199–210
35. Shabana YM, Noda N (2001) Thermo-elasto-plastic stresses in functionally graded materials subjected to thermal loading taking residual stresses of the fabrication process into consideration. Compos Part B 32(2):111–121
36. Grujicic M, Zhao H (1998) Optimization of 316 stainless steel/alumina functionally graded material for reduction of damage induced by thermal residual stresses. Mater Sci Eng A 252(1):117–132
37. Becker TL Jr, Cannon RM, Ritchie RO (2000) An approximate method for residual stress calculation in functionally graded materials. Mech Mater 32(2):85–97
38. Lee CS, Ahn S-H, DeJonghe LC, Thomas G (2006) Effect of functionally graded material (FGM) layers on the residual stress of polytypoidally joined Si3N4–Al_2o_3. Mater Sci Eng A A 434(1–2):160–165
39. Wei X, Chen W, Chen B (2015) Minimizing Thermal Residual Stress in Ni/Al_2o_3 Functionally Graded Material Plate by Volume Fraction Optimization. Cmc-Computers Materials Continua 48(1):1–23
40. Dancer CEJ, Achintha M, Salter CJ, Fernie JA, Todd RI (2012) Residual stress distribution in a functionally graded alumina–silicon carbide material. Scr Mater 67(3):281–284
41. Ding S, Wu C-P (2018) Optimization of material composition to minimize the thermal stresses induced in FGM plates with temperature-dependent material properties. Int J Mech Mater Des 14(4):527–549
42. Parihar RS, Setti SG, Sahu RK (2019) Prediction of thermal residual stresses in sigmoid functionally graded materials. In: AIP Conference Proceedings, vol. 2148, no. 1, p. 030018. AIP Publishing LLC
43. Shi JM, Ma N, Zhang LX, Feng JC (2018) Residual stress and fracture strength of brazed joint of ceramic and titanium alloy with the aid of laser deposited functionally graded material layers. J Manuf Process 34:495–502
44. Alexandrov, Sergei, Elena Lyamina, and V. Nguyen Khoa. "Distribution of Stresses and Residual Stresses in FGM Discs Subject to Internal Pressure." In Proceedings of the 2018 International Conference on Mechatronic Systems and Robots, pp. 51–55. 2018
45. Strashnov S, Alexandrov S, Lang L (2019) Description of residual stress and strain fields in FGM hollow disc subject to external pressure. Materials 12(3):440
46. Wagih A, Fathy A (2017) Experimental investigation and FE simulation of spherical indentation on nano-alumina reinforced copper-matrix composite produced by three different techniques. Adv Powder Technol 28(8):1954–1965
47. Eltaher MA, Wagih A, Melaibari A, Fathy A, Lubineau G (2020) Effect of Al_2o_3 particles on mechanical and tribological properties of Al–Mg dual-matrix nanocomposites. Ceram Int 46(5):5779–5787
48. Fathy A, Abu-Oqail A, Wagih A (2018) Improved mechanical and wear properties of hybrid Al-Al_2o_3/GNPs electro-less coated Ni nanocomposite. Ceram Int, 22145 44(18):22135
49. Wagih A, Fathy A (2018) Improving compressibility and thermal properties of Al–Al_2o_3 nanocomposites using Mg particles. J Mater Sci 53(16):11393–11402
50. Abd-Elwahed MS, Meselhy AF (2020) Experimental investigation on the mechanical, structural and thermal properties of cu–ZrO2 nanocomposites hybridized by graphene nanoplatelets. Ceram Int
51. Sadoun AM, Fathy A, Abu-Oqail A, Elmetwaly HT, Wagih A (2020) Structural, mechanical and tribological properties of Cu–ZrO2/GNPs hybrid nanocomposites. Ceram Int 46(6):7586–7594
52. Sadoun, A. M., and A. Fathy. "Experimental study on tribological properties of Cu–Al_2o_3 nanocomposite hybridized by graphene nanoplatelets." Ceram Int 45, no. 18 (2019): 24784–24792
53. Abu-Oqail A, Samir A, Essa ARS, Wagih A, Fathy A (2019) Effect of GNPs coated Ag on microstructure and mechanical properties of cu-Fe dual-matrix nanocomposite. J Alloys Compd 781:64–74
54. Wagih, A., A. Abu-Oqail, and A. Fathy. "Effect of GNPs content on thermal and mechanical properties of a novel hybrid Cu-Al_2o_3/GNPs coated Ag nanocomposite." Ceram Int 45, no. 1 (2019): 1115–1124
55. Aghaei M, Nazari F, Honarpisheh M (2019) Effect of cooling system on the mechanical properties and residual stress of steel AISI 1045 in quenching heat treatment. Modares Mechanical Eng 19(12):2979–2986
56. Nazari F, Honarpisheh M, Zhao H (2019) Effect of stress relief annealing on microstructure, mechanical properties, and residual stress of a copper sheet in the constrained groove pressing process. Int J Adv Manuf Technol 102(9–12):4361–4370
57. Prime MB (2001) Cross-sectional mapping of residual stresses by measuring the surface contour after a cut. J Eng Mater Technol 123(2):162–168
58. Moazam MA, Honarpisheh M (2019) Residual stress formation and distribution due to precipitation hardening and stress relieving of AA7075. Mater Res Express 6, no. 12:126108
59. Turski M, Edwards L (2009) Residual stress measurement of a 316l stainless steel bead-on-plate specimen utilising the contour method. Int J Press Vessel Pip 86(1):126–131